ARTICLES

Quantum Dynamics Study on the Product Branching for the $C(^3P) + C_2H_2$ Reaction: *cyclic*-C_3H versus *linear*-C_3H†

Toshiyuki Takayanagi*

Department of Chemistry, Saitama University, 255 Shimo-Okubo, Sakura-ku, Saitama City, Saitama 338-8570, Japan

Received: January 5, 2005; In Final Form: February 11, 2005

Reduced-dimensionality quantum reactive scattering calculations for the $C(^3P) + C_2H_2$ reaction have been carried out in order to understand the product branching dynamics of *cyclic*-C_3H + H and *linear*-C_3H + H. Our model treats only two degrees of freedom but can explicitly describe both of the C_3H isomer product channels. The lowest triplet potential energy surface has been obtained by the hybrid density-functional method at the B3LYP/6-31G(d,p) level of theory. The calculated reaction probabilities were found to be dominated by resonance consistent with the complex-formation potential, and the results show that *cyclic*-C_3H is preferentially formed via the *cyclic*-C_3H_2 intermediate produced by insertion of $C(^3P)$ into the CC bond. We have found that the isomerization from the *cyclic*-C_3H_2 to *linear*-C_3H_2 intermediate is suppressed by a barrier separating potential wells corresponding to these two intermediates. It has also been found that the energy dependence of the calculated total reaction cross section is in good agreement with the result of crossed molecular beam experiments.

1. Introduction

The reaction of the ground-state atomic carbon $C(^3P)$ with unsaturated hydrocarbons has recently attracted considerable interest due to its fundamental importance in the chemistry of dense interstellar clouds.[1,2] It has been proposed that these reactions are key steps for the synthesis of large carbon-containing species. The importance of these reactions in the interstellar clouds has primarily been pointed out by rate constant measurements at low temperatures in the range 10−50 K. It has been found that these reactions are very fast even at 15 K and that they have a weak negative temperature dependence. This indicates that these reactions do not have a barrier in the entrance region of the potential energy surface. To understand the whole chemistry of interstellar clouds, it is also important to know not only overall rate constants at low temperatures but also reaction products. Since the kinetic studies generally measure the disappearance of reactant molecules, those studies cannot identify the reaction products. Alternatively, crossed molecular beam experiments are quite useful, although a mass spectroscopic technique, which is frequently used in such experiments, generally cannot distinguish isomers.

The reaction of $C(^3P)$ with acetylene is the simplest one in this class and has been extensively studied from both the theoretical and experimental points of view. The rate constant at room temperature for this reaction was reported to be very large, suggesting no barrier in the potential energy surface of the $C(^3P) + C_2H_2$ reaction.[3−5] The kinetic measurement was further extended down to the temperature range 300−15 K,[6,7]

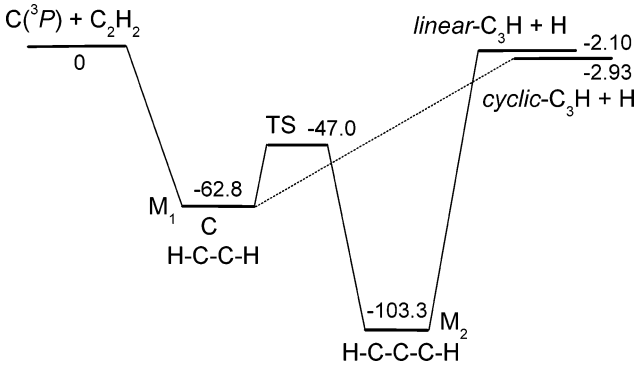

Figure 1. Schematic energy diagram (in kilocalories per mole) of the $C(^3P) + C_2H_2$ reactants, intermediates, and C_3H + H products on the lowest triplet potential energy surface obtained at the B3LYP/6-31G-(d,p) level of theory.

and it has been found that the rate constant has a negative temperature dependence and that the absolute value of the rate constant is very large ($>2 \times 10^{-10}$ cm^3 molecule^{-1} s^{-1}) even at 15 K. A simplified schematic energy diagram of the $C(^3P) + C_2H_2$ reaction obtained from the B3LYP/6-31G(d,p) electronic structure calculations[8] is presented in Figure 1. This reaction energetically leads to the production of two C_3H isomers: *cyclic*-C_3H and *linear*-C_3H. Kaiser and co-workers[9−11] have performed an extensive series of crossed molecular beam experiments at relatively high collision energies. They concluded that the *cyclic*-C_3H molecule is preferentially produced with a minor contribution of the *linear*-C_3H product at higher collision energies from the obtained angular distributions. A more recent crossed molecular beam experiment[12] indicates that $C(^3P) +$

† Part of the special issue "Donald G. Truhlar Festschrift".

* E-mail: tako@chem.saitama-u.ac.jp.

10.1021/jp0510037 CCC: $33.50
Published on Web 05/14/2005

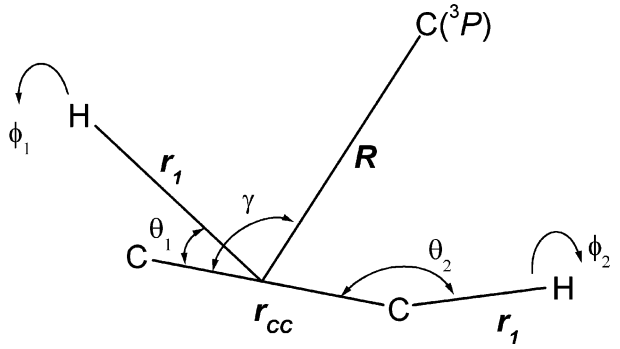

Figure 2. Coordinate system used for constructing reduced-dimensionality potential energy surfaces. R and r_1 were taken as active coordinates in quantum scattering calculations.

C_2H_2 also leads to $C_3(^1\Sigma_g^+)$ + H_2 products through the spin-forbidden intersystem-crossing mechanism.

On the theoretical side, electronic structure calculations for the $C(^3P)$ + C_2H_2 reaction at various levels of theory have been extensively carried out so far.[8,10,11,13−17] In addition, Buonomo and Clary[17] have recently reported a quantum dynamics study for the first time. They have treated the $C(^3P)$ + C_2H_2 reaction with a reduced-dimensionality model, in which two degrees of freedom, the distance R between $C(^3P)$ and the center of mass of C_2H_2 and the angle R makes with the C_2H_2 bond axis, are taken into account in the dynamics. They developed a two-dimensional potential energy surface based on the ab initio CCSD(T) electronic structure calculations with the other seven degrees of freedom being optimized. They have then performed two-dimensional time-dependent wave packet calculations to obtain reaction probabilities. Although the wave packet calculations were carried out only in the entrance region of the potential energy surface, they were able to obtain the information about the *cyclic*-C_3H/*linear*-C_3H product branching by changing the location of the flux absorbing potentials. They have found that *linear*-C_3H is formed preferentially, while the *cyclic*-C_3H product contributes at higher collision energies. Clearly, this result contradicts an interpretation of the crossed molecular beam experiments.[9−11]

Motivated by these studies as mentioned above, we here present quantum reactive scattering calculations based on a different reduced-dimensionality model from the model of Buonomo and Clary.[17] Our reduced-dimensionality model is quite simple and a minimal one, but it can explicitly describe both the *cyclic*-C_3H and *linear*-C_3H production channels without a flux absorption technique. We believe that the present study is a good starting point for future theoretical developments to fully understand the mechanism and dynamics of the $C(^3P)$ + C_2H_2 reaction.

2. Method of Calculations

The coordinate system used in this study is displayed in Figure 2. Since the C + C_2H_2 reaction system includes five atoms, the system has then nine degrees of freedom. In the present dynamics study, only two coordinates are taken into account in dynamics calculations, the distance between $C(^3P)$ and the midpoint of CC of acetylene and the distance between H and the midpoint of CC. The other seven degrees of freedom have been optimized with respect to the total electronic energy. Zero-point vibrational energies have not explicitly been included due to the computational cost of electronic structure calculations. However, their effect on the potential energy surface is not expected to be large. Notice that these two coordinates are a minimal set that can describe both the C + C_2H_2 reactants and the C_3H + H products and this simplified model may be a good starting point to understand the product branching dynamics. Soon, we will add more degrees of freedom in dynamics calculations in order to understand the validity of the present two-degrees-of-freedom model.

The Hamiltonian of the present system can approximately be written by

$$H = -\frac{\hbar^2\partial^2}{2\mu\partial R^2} - \frac{\hbar^2\partial^2}{2\mu'\partial r_1^{\,2}} + \frac{\hbar^2}{2\mu R^2}l(l+1) + V_{\text{eff}}(R,r_1)$$

where μ and μ' are the reduced masses of the corresponding relative motions, V_{eff} is the effective potential energy interaction as a function of the two coordinates, and l is the collisional angular momentum quantum number. In this model, notice that the value of l is conserved during the reactive collision also in the product region. Since the rotational motion of the reactant C_2H_2 is completely ignored in our dynamics model, it assumes that the initial orbital angular momentum is adiabatically converted into the rotational angular momentum of the product C_3H molecule. This may be presumably a good approximation because a heavy carbon atom is initially attached to C_2H_2 and then a light hydrogen atom is finally released.

The scattering problem has been solved by both time-independent and time-dependent methods.[18] The time-independent close-coupling method has been mainly used for calculating reaction probabilities as well as reactive cross sections. We have employed a standard hyperspherical close-coupling method after converting the (R, r_1) coordinates into the (ρ, θ) polar coordinates, where a one-dimensional eigenvalue problem along θ at a given value of ρ was solved by the standard discrete-variable-representation method,[19] with the particle-in-box basis set. The number of the basis set was chosen to be 1000 from convergence tests. The resulting close-coupling equations using the lowest 50 states were solved by the standard R-matrix propagation method[20] in the range 0.5 Å $\le \rho \le$ 13 Å (divided in about 500 sectors), and then state-to-state reaction probabilities were obtained. Calculations have been carried out in the range of angular momentum between 1 and 120, with a step of $\delta l = 1$. Since we did not use the flux absorbing potential in the time-independent calculations, note that the lowest value of l was set to 1 to avoid the $R \sim 0$ region.

The time-dependent wave packet method has also been used for qualitative understanding of the reaction mechanism. In this case, the coordinate system remains the same but the wave packet was propagated in time by the standard split-operator method.[18] We employed the fast-Fourier transform method to evaluate the action of the kinetic energy operator on the wave packet, where 512 grid points were used for both R and r_1 in the range 0 Å $\le R \le$ 6.5 Å and 1.2 Å $\le r_1 \le$ 7.5 Å. The initial wave function is given by the product of a pure vibrational eigenstate along the r_1 coordinate and a Gaussian translational wave packet, where appropriate parameters for the starting point and the energy distribution width of the wave packet were chosen. After passing the dividing lines defining the reactant and products, the wave packet was absorbed by a negative imaginary potential to prevent reflection from the grid boundary. The wave packet propagation was carried out up to $t \sim 2.5$ ps, so that the wave packet density was decreased to zero.

We employed the hybrid density-functional B3LYP/6-31G-(d,p) level[21] for all electronic structure calculations presented in this paper. A simplified schematic energy diagram obtained at this level of theory is already shown in Figure 1. Needless to say, it is highly desirable that one should employ a high-level

electronic structure theory in order to obtain an accurate global potential energy surface of a reaction system. One of the important properties of the potential surface is the exothermicity of the reaction system. In the case of the $C(^3P) + C_2H_2 \rightarrow$ *linear*-C_3H/*cyclic*-$C_3H + H$ reaction, it has been found that the reaction exothermicity is strongly sensitive to the level of electronic structure theory. Previous ab initio calculations[13] show that the *linear*-C_3H molecule has a $^2\Pi$-like character. This indicates that the single-reference Hartree−Fock method cannot give reliable total electronic energies due to the spin-contamination problem. It has been known that the MP*n* level calculations based on the single-reference Hartree−Fock molecular orbitals also do not yield reliable energetics.[14] To obtain reliable results for this reaction, one has to employ more accurate levels of theory such as the MRCI and CCSD(T) methods. However, electronic structure calculations using these methods are very time-consuming processes, since a large number of the geometry optimization steps should be carried out to even obtain a reduced-dimensionality potential energy surface. After testing various electronic structure levels of theory, we have noticed that the hybrid density-functional B3LYP method gives reasonable reaction energetics at a reasonable computational cost. As shown in Figure 1, the B3LYP/6-31G(d,p) calculation gives reaction exothermicities for the *linear*-$C_3H + H$ and *cyclic*-$C_3H + H$ channels of +2.10 and +2.93 kcal/mol, respectively, without zero-point vibrational energy corrections. These values are somewhat larger than the corresponding MRCI and CCSD(T) results, but the stability order of *linear*-C_3H and *cyclic*-C_3H at the B3LYP/6-31G(d,p) level is in agreement with the more accurate MRCI/cc-pVTZ[13] and CCSD(T)/QZ2P[14] results. For the relative energies of the intermediates, it seems that the B3LYP/6-31G(d,p) level calculations give somewhat larger stabilization energies with respect to the reactants. For example, the *cyclic*-C_3H_2 (cyclopropenylidene, M_1) and *linear*-C_3H_2 (propargylene, M_2) have energies of −62.8 and −103.3 kcal/mol with respect to the reactants at the B3LYP/6-31G(d,p) level of theory. These values are −53.8 and −92.3 kcal/mol, respectively, at the CCSD(T)/QZ2P level of theory.[14]

Before presenting a global reduced-dimensionality potential energy surface, we first report the potential energy curves for the hydrogen atom dissociation processes of the *cyclic*-C_3H_2 and *linear*-C_3H_2 intermediates, since the main focus of this paper is to understand the production dynamics of the $C(^3P) + C_2H_2$ reaction. Figure 3 shows the plot of the total electronic energies as a function of the C−H distance for both the *cyclic*-$C_3H_2 \rightarrow$ *cyclic*-$C_3H + H$ and *linear*-$C_3H_2 \rightarrow$ *linear*-$C_3H + H$ processes, where the other eight internal coordinates were optimized with respect to the total energy. Note that there is no barrier for both of the dissociation processes. A similar plot was previously reported by Takahashi and Yamashita[13] with the CASSCF/D95V(d,p) level of theory. Interestingly, they have found a small barrier of about 3 kcal/mol for the *linear*-$C_3H_2 \rightarrow$ *linear*-$C_3H + H$ dissociation process but no barrier for the *cyclic*-$C_3H_2 \rightarrow$ *cyclic*-$C_3H + H$, although they failed to perform complete geometry optimizations for the former process due to the floppiness of the molecule. They have concluded that a small barrier along this pathway exists even if other internal coordinates were fully relaxed.

Figure 4 shows the two-dimensional contour plot of the potential energy surface as a function of R and r_1 with the other seven internal coordinates being optimized with respect to energy. This potential surface was constructed with the standard two-dimensional spline interpolation method based on about 1000 point calculations. Specifically, we have carried out the

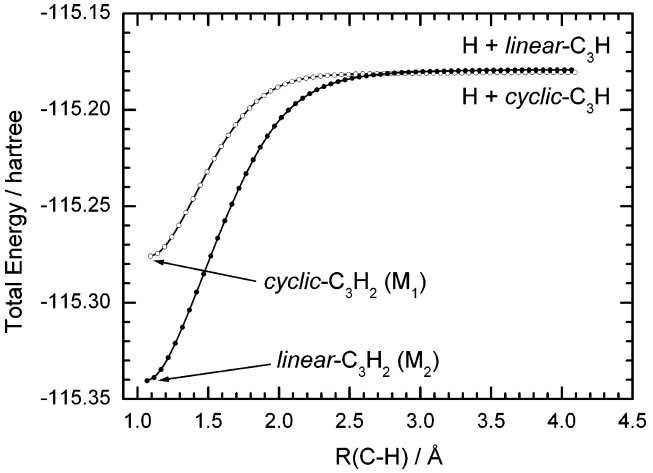

Figure 3. Potential energy curves for *cyclic*-$C_3H_2 \rightarrow$ *cyclic*-$C_3H + H$ (open circles) and *linear*-$C_3H_2 \rightarrow$ *linear*-$C_3H + H$ (solid circles) as a function of the C−H internuclear distance calculated at the B3LYP/6-31G(d,p) level of theory. The other eight internal coordinates are optimized with respect to total energy.

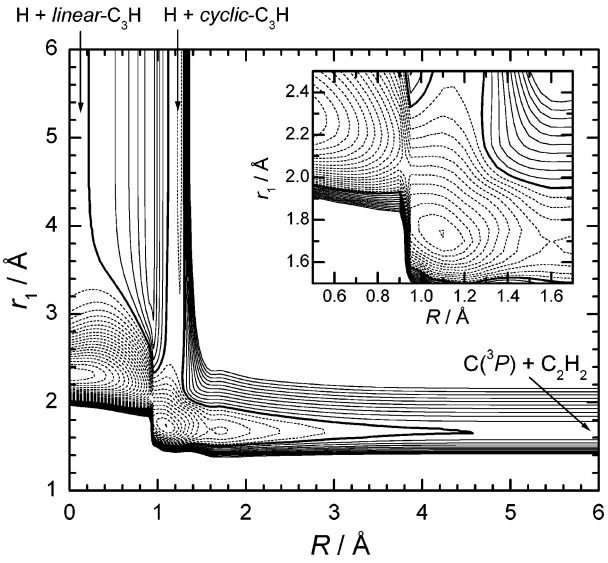

Figure 4. Contour plot of the potential energy surface for the $C(^3P) + C_2H_2 \rightarrow$ *cyclic*-C_3H/*linear*-$C_3H + H$ reaction as a function of R and r_1 calculated at the B3LYP/6-31G(d,p) level. Zero of the energy is take to be the reactant minimum. Contours are spaced by 5 kcal/mol; solid lines are used for energies that are positive relative to $C(^3P) + C_2H_2$, dashed lines are used for negative energies, and the bold line denotes the zero contour.

B3LYP/6-31G(d,p) calculations with a very small step (∼0.05−0.1 Å) in a strong interaction region of 0 Å < R < 2 Å and 1.4 Å < r_1 < 2.4 Å in order to obtain a potential energy surface smooth enough for the dynamical use. In other regions, a somewhat large step size (∼0.1−0.2 Å) was employed. It is seen that there is no barrier in the $C + C_2H_2$ entrance region similar to the previous ab initio calculations of Buonomo and Clary at the RCCSD(T)/cc-pVDZ level.[17] However, it is expected that their ab initio results give a more accurate long-range attractive interaction, since it is well-known that the B3LYP method cannot often describe accurate long-range interactions. We can see a potential well around $R \sim 1.1$ Å corresponding to the *cyclic*-C_3H_2 intermediate (M_1), while a deep well around $R \sim 0$ Å corresponds to the *linear*-C_3H_2 intermediate (M_2). There exists a barrier at $R \sim 0.95$ Å separating these two potential wells. For large values of r_1, two product valleys are clearly seen at $R \sim 0$ Å and $R \sim 1.2$ Å. The former valley

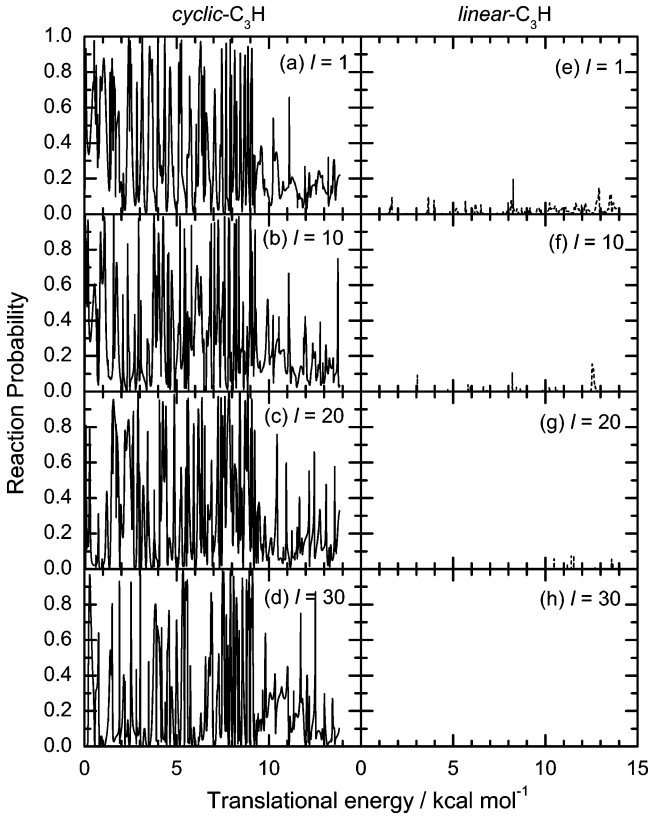

Figure 5. Reaction probabilities for the $C(^3P) + C_2H_2 \rightarrow$ *cyclic*-$C_3H + H$ reaction (left panels) and for $C(^3P) + C_2H_2 \rightarrow$ *linear*-$C_3H + H$ (right panels) as a function of the translational energy for some values of the angular momentum quantum number (l).

corresponds to the *linear*-$C_3H + H$ production channel, while the latter, to the *cyclic*-$C_3H + H$ channel. Therefore, the present two-degrees-of-freedom model can qualitatively describe the branching dynamics of these two production channels.

3. Results and Discussion

Figure 5 shows the reaction probabilities for both the $C(^3P) + C_2H_2(v = 0) \rightarrow$ *cyclic*-$C_3H + H$ and $C(^3P) + C_2H_2 \rightarrow$ *linear*-$C_3H + H$ processes as a function of the translational energy obtained from the time-independent quantum scattering calculations for some selected values of the collisional angular momentum quantum number (l). It can be seen that the calculated reaction probabilities are generally dominated by resonance. This resonance feature can easily be understood from the reaction mechanism presented in Figure 1 as well as the topological feature of the potential energy surface shown in Figure 4, indicating the existence of long-lived quasibound intermediates on the lowest triplet potential energy surface. In addition, it is interesting to note that resonance peaks are not completely isolated but significantly overlap in this energy region. This suggests that a resonance feature may presumably become broader if we include more degrees of freedom in quantum dynamics calculations.

The most important point which should be noticed from Figure 5 is that the probability to produce *linear*-C_3H is much smaller than that for the *cyclic*-C_3H production. This is an unexpected result because the present potential energy surface has a deep potential well corresponding to the *linear*-C_3H_2 intermediate. If this intermediate would efficiently be produced during collision, it is expected that we would observe a significant probability for the *linear*-C_3H production channel,

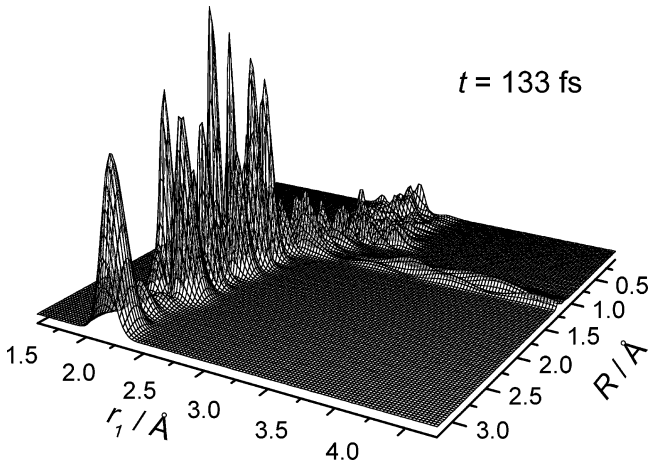

Figure 6. Three-dimensional perspective plot of the probability density of the wave packet as a function of R and r_1 for $l = 0$ after 133 fs of propagation.

since the exit energy levels of the *cyclic*-$C_3H + H$ and *linear*-$C_3H + H$ channels are comparable. The present result is thus highly in contrast to the reduced-dimensionality wave packet result of Buonomo and Clary.[17] As mentioned in the Introduction, they have developed a different reduced-dimensionality model, where the distance R and orientation angle of the approaching carbon atom with respect to acetylene (γ in Figure 2) were taken into account in the dynamics. They have calculated the *cyclic*-C_3H/*linear*-C_3H branching ratio by changing the location of the flux absorbing potential and found that *linear*-C_3H is preferentially formed, although they have also observed an increasing contribution of the *cyclic*-C_3H production as the energy increases. Since their model includes the γ-coordinate dynamics, their model can describe the sideways addition mechanism to finally form *linear*-C_3H via the *s*-trans prodendiylene intermediate, whereas this process is completely ignored, since the γ-coordinate is optimized in our reduced-dimensionality model. Buonomo and Clary have found that this sideways pathway equally contributes to the overall *linear*-C_3H formation. Therefore, it is reasonable that our reduced-dimensionality model significantly underestimates the *linear*-C_3H formation probability.

To qualitatively understand the small probability for the $C(^3P) + C_2H_2 \rightarrow$ *linear*-$C_3H + H$ reaction, we have performed time-dependent wave packet calculations. The center of the initial Gaussian wave packet was located at $R = 4$ Å, and the translational energy distribution was centered at $E_t = 2.3$ kcal/mol. Figure 6 displays a representative three-dimensional perspective plot of the probability density distribution of the wave packet after 133 fs of propagation for $l = 1$. Once the wave packet reaches the strong interaction region ($t \sim 100$ fs), an essential feature of the wave packet remains the same as this figure, although the magnitude of the probability density gradually decreases as the time increases, since the wave packet is absorbed both at the reactant and product edges. From this figure, it can be seen that the *cyclic*-C_3H molecule is more preferentially produced than *linear*-C_3H. As shown in Figure 5, the $C(^3P) + C_2H_2$ reaction is resonance-dominated within a framework of the present two-dimensional model, and the result of Figure 6 thus indicates that the resonance wave function is dominantly located between the $C(^3P) + C_2H_2$ reactant region and the *cyclic*-C_3H_2 intermediate region. It can be seen that a part of the wave packet is localized in the *linear*-C_3H_2 intermediate region, but its contribution was seen to be relatively small. This fact suggests that the barrier separating the *cyclic*-

C_3H_2 and *linear*-C_3H_2 potential wells plays an important role and prevents the isomerization from *cyclic*-C_3H_2 to *linear*-C_3H_2. In other words, the energy along the *R* coordinate may not be efficiently converted into the energy overcoming the barrier. This can be qualitatively understood from the characteristics of the present two-dimensional potential energy surface around the barrier region (see the inserted contour plot in Figure 4); however, this mechanism is also in contrast with the wave packet result of Buonomo and Clary.[17] They have found that, once the *cyclic*-C_3H_2 intermediate is initially formed, it readily converts into the *linear*-C_3H_2 intermediate by surmounting the barrier and then finally produces *linear*-C_3H + H. This disagreement partly comes from the fact that the present reaction mechanism is completely resonance-dominated within our two-dimensional model. To understand the reason for this discrepancy, it should be interesting to carry out quantum scattering calculations including the contribution of the γ-coordinate (see Figure 2). This would be an important future problem. Alternatively, it is interesting to perform a classical dynamics calculation treating all degrees of freedom on an accurate potential energy surface. This would also be another important issue and is currently in progress in our research group.

From the angular momentum dependence of the reaction probability shown in Figure 5, it is found that the $C(^3P) + C_2H_2 \rightarrow$ *cyclic*-C_3H + H reaction probability remains similar as *l* increases from $l = 1$ to $l = 30$ but that the $C(^3P) + C_2H_2 \rightarrow$ *linear*-C_3H + H reaction probability considerably decreases as *l* increases. This *l* dependence of the reaction probability was previously discussed by Buonomo and Clary in detail.[17] As shown in Figure 4, the *linear*-C_3H_2 minimum is located around small values of *R* ($\sim$0 Å), while the *cyclic*-C_3H_2 local minimum is located at an outer region of $R \sim 1.1$ Å. In addition, a barrier separating these wells at $R \sim 0.95$ Å exists. If the effect of the centrifugal potential is taken into account, for larger values of *l*, the total potential energies will be shifted to higher energies more significantly for the *linear*-C_3H_2 minimum region than the *cyclic*-C_3H_2 minimum region. Notice that the barrier between these wells is also shifted to a higher energy as *l* increases. Therefore, the incoming wave packet will be blocked by this barrier for larger *l* values and thus the *linear*-C_3H_2 intermediate region cannot be accessible for larger *l* values. A simple analysis of the effective potential energy curve shows that the *linear*-C_3H_2 intermediate cannot be formed at $l \sim 50$ in the translational energy range considered in this work. On the other hand, in the case of the *cyclic*-C_3H_2 intermediate, the reaction can occur up to $l \sim 100$. Thus, the trend of the reaction probability for $C(^3P) + C_2H_2 \rightarrow$ *cyclic*-C_3H + H is quite similar in the range from $l = 1$ to $l = 30$, as shown in Figure 5.

Figure 7 displays the cross sections for the $C(^3P) + C_2H_2 \rightarrow$ *cyclic*-C_3H + H and $C(^3P) + C_2H_2 \rightarrow$ *linear*-C_3H + H reactions obtained in the present study as a function of the translational energy. Since the cross section for the *linear*-C_3H production is too small to be seen in the linear plot of Figure 7a, the logarithmic plot of the cross sections is also shown in Figure 7b. The cross section for the *cyclic*-C_3H production decreases with the energy increases, and this behavior is consistent with the barrierless reaction. From the result of Figure 7b, the cross section of the *linear*-C_3H production is much smaller than that of the *cyclic*-C_3H production by a factor of 10^2-10^4 in this energy range. Figure 8 displays the branching fraction of the *linear*-C_3H production as a function of the translational energy. It is interesting to note that the fraction to produce *linear*-C_3H gradually increases as the energy increases, although the absolute value is quite small. This result suggests that the isomerization

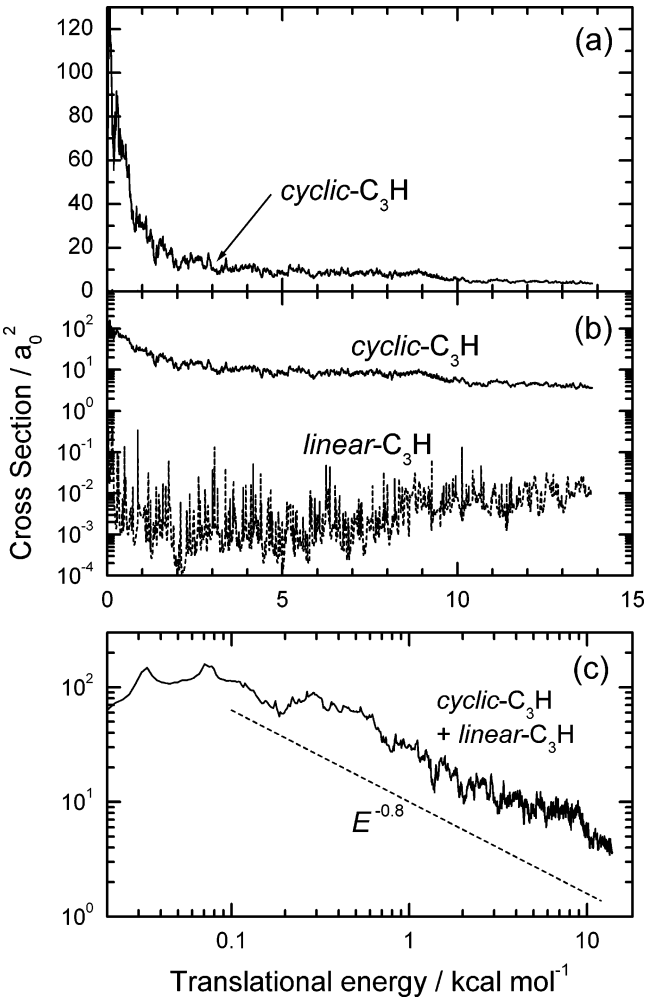

Figure 7. Calculated cross sections for the $C(^3P) + C_2H_2 \rightarrow$ *cyclic*-C_3H/*linear*-C_3H + H reaction as a function of the translational energy. The dashed line in part c indicates the $E^{-0.8}$ dependence obtained from the crossed molecular beam experiments of ref 12.

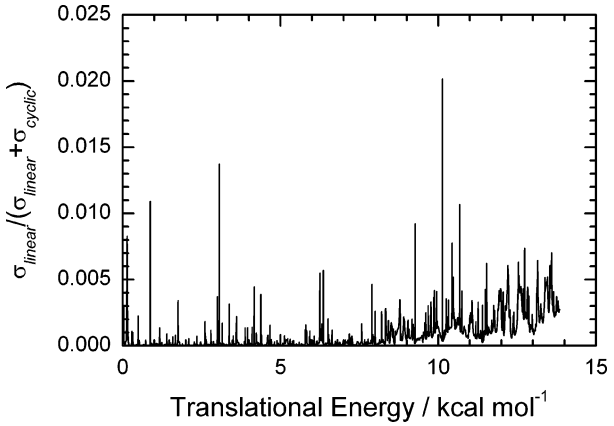

Figure 8. Branching fraction for the formation of *cyclic*-C_3H and *linear*-C_3H as a function of the translational energy.

probability from the *cyclic*-C_3H_2 to the *linear*-C_3H_2 intermediate increases with the increase in energy, as suggested previously. In Figure 7c, we compare the energy dependence of the cross section with the experimental result in a log−log plot. The previous molecular beam experiment[12] shows the $E^{-0.8}$ dependence in the translational energy range 0.07−4.8 kcal/mol, although only relative cross sections have been reported. It is easily suggested that the absolute value of the cross section calculated in the present study is not reliable because only two

degrees of freedom were taken into account in the dynamics and the entrance attractive potential was based on the inaccurate B3LYP electronic structure calculations. In fact, the present cross section is smaller by a factor of 3−4 than that from the quantum dynamics results of Buonomo and Clary[17] who employed a more accurate long-range attractive potential based on the RCCSD(T) calculations. Nevertheless, it is interesting that the energy dependence obtained in this study fairly agrees with the result of molecular beam experiments.

4. Conclusions

Reduced-dimensionality quantum reactive scattering calculations have been performed for the $C(^3P) + C_2H_2$ reaction in order to understand the product branching dynamics: *cyclic*-$C_3H + H$ versus *linear*-$C_3H + H$. Only two degrees of freedom were taken into account in the dynamics, and this two-dimensional model is the minimal one that can explicitly describe both the reactant channel and two production channels without a flux absorbing technique. We found that the calculated reaction probability is dominated by a sharp resonance feature and that this result is consistent with the existence of two deep potential wells corresponding to the *cyclic*-C_3H_2 and *linear*-C_3H_2 intermediates. However, it has been found that *cyclic*-C_3H is dominantly produced via the *cyclic*-C_3H_2 intermediate. Time-dependent wave packet calculations revealed that a barrier separating the *cyclic*-C_3H_2 and *linear*-C_3H_2 intermediate wells play an important role in the product branching dynamics. The minority of the *linear*-C_3H product is partly due to the fact that the present reduced-dimensionality model does not take the sideways addition mechanism into account. Additional quantum dynamics studies including the motion of the $C-C_2H_2$ orientation angle degree of freedom are needed to understand the product branching dynamics of the $C(^3P) + C_2H_2$ reaction more quantitatively. The translational energy dependence of the calculated reaction cross section has also been compared to the result of previous crossed molecular beam experiments. Although the absolute value of the calculated cross section seems to be small, the energy dependence has been found to be in good agreement with the experimental result.

Clearly, additional theoretical studies are necessary to fully understand the mechanism and dynamics of the $C(^3P) + C_2H_2$ reaction. For example, classical trajectory calculations treating all degrees of freedom will be quite useful with a direct dynamics technique. In addition, the effect of electronically nonadiabatic transitions between triplet and singlet states should be investigated, since the spin-forbidden $C_3(^1\Sigma) + H_2$ products have experimentally been identified. We believe that the reaction dynamics methods will be quite useful for understanding the chemistry of interstellar clouds.

References and Notes

(1) Clary, D. C.; Buonomo, E.; Sims, I. R.; Smith, I. W. M.; Geppert, W. D.; Naulin, C.; Costes, M.; Cartechini, L.; Casavecchia, P. *J. Phys. Chem. A* **2002**, *106*, 5541.
(2) Smith, I. W. M. *Chem. Soc. Rev.* **2003**, *31*, 137.
(3) Haider, N.; Husain, D. *Z. Phys. Chem*. (*Munich*) **1992**, *176*, 133.
(4) Haider, N.; Husain, D. *J. Chem. Soc., Faraday Trans*. **1993**, *89*, 7.
(5) Clary, D. C.; Haider, N.; Husain, D.; Kabir, M. *Astrophys. J*. **1994**, *422*, 416.
(6) Chastaing, D.; James, P. L.; Le Picard, S. D.; Sims, I. R.; Smith, I. W. M. *Phys. Chem. Chem. Phys*. **1999**, *1*, 2247.
(7) Chastaing, D.; Le Picard, S. D.; Sims, I. R.; Smith, I. W. M. *Astron. Astrophys*. **2001**, *365*, 241.
(8) Takayanagi, T. *Chem. Phys.* **2005**, *312*, 61.
(9) Kaiser, R. I.; Stranges, D.; Lee, Y. T.; Suits, A. G. *Astrophys. J*. **1997**, *477*, 982.
(10) Kaiser, R. I.; Ochsenfeld, C.; Head-Gordon, M.; Lee, Y. T.; Suits, A. G. *J. Chem. Phys*. **1997**, *106*, 1729.
(11) Kaiser, R. I.; Mebel, A. M.; Lee, Y. T. *J. Chem. Phys*. **2001**, *114*, 231.
(12) Cartechini, L.; Bergeat, A.; Capozza, G.; Casavecchia, P.; Volpi, G. G.; Geppert, W. D.; Naulin, C. Costes, M. *J. Chem. Phys*. **2002**, *116*, 5603.
(13) Takahashi, J.; Yamashita, K. *J. Chem. Phys.* **1996**, *104*, 6614.
(14) Ochsenfeld, C.; Kaiser, R. I.; Lee, Y. T.; Suits, A. G.; Head-Gordon, M. *J. Chem. Phys*. **1997**, *106*, 4141.
(15) Guadagnini, R.; Schatz, G. C.; Walch, S. P. *J. Phys. Chem. A* **1998**, *102*, 5857.
(16) Mebel, A. M.; Jackson, W. M.; Chang, A. H. H.; Lin, S. H. *J. Am. Chem. Soc*. **1998**, *120*, 5751.
(17) Buonomo, E.; Clary, D. C. *J. Phys. Chem. A* **2001**, *105*, 2694.
(18) Nyman, G.; Yu, H.-G. *Rep. Prog. Phys.* **2001**, *63*, 1001.
(19) Light, J. C.; Hamilton, I. P.; Lill, J. V. *J. Chem. Phys*. **1985**, *82*, 1400.
(20) Light, J. C.; Walker, R. B. *J. Chem. Phys*. **1976**, *65*, 4272.
(21) Frisch, M. J.; Trucks, G. W.; Schlegel, H. B.; Scuseria, G. E.; Robb, M. A.; Cheeseman, J. R.; Zakrzewski, V. G.; Montgomery, J. A., Jr.; Stratmann, R. E.; Burant, J. C.; Dapprich, S.; Millam, J. M.; Daniels, A. D.; Kudin, K. N.; Strain, M. C.; Farkas, O.; Tomasi, J.; Barone, V.; Cossi, M.; Cammi, R.; Mennucci, B.; Pomelli, C.; Adamo, C.; Clifford, S.; Ochterski, J.; Petersson, G. A.; Ayala, P. Y.; Cui, Q.; Morokuma, K.; Malick, D. K.; Rabuck, A. D.; Raghavachari, K.; Foresman, J. B.; Cioslowski, J.; Ortiz, J. V.; Baboul, A. G.; Stefanov, B. B.; Liu, G.; Liashenko, A.; Piskorz, P.; Komaromi, I.; Gomperts, R.; Martin, R. L.; Fox, D. J.; Keith, T.; Al-Laham, M. A.; Peng, C. Y.; Nanayakkara, A.; Challacombe, M.; Gill, P. M. W.; Johnson, B.; Chen, W.; Wong, M. W.; Andres, J. L.; Gonzalez, C.; Head-Gordon, M.; Replogle, E. S.; Pople, J. A. Gaussian 98, revision A.9; Gaussian, Inc.: Pittsburgh, PA, 1998.